Available online at www.sciencedirect.com
ScienceDirect
Analytica Chimica Acta 598 (2007) 147–154
ANALYTICA CHIMICA ACTA
www.elsevier.com/locate/aca

A dual detector capillary waveguide biosensor for detection and quantification of hybridized target

Harbans S. Dhadwal [a,*], Bhaskar Mukherjee [a], Paul Kemp [b], Josephine Aller [b], Yuan Liu [b], JoAnn Radway [b]

[a] *Department of Electrical and Computer Engineering, Stony Brook University, Stony Brook, NY 11794, United States*
[b] *School Marine and Atmospheric Sciences, Stony Brook University, Stony Brook, NY 11794, United States*

Received 11 May 2007; received in revised form 10 July 2007; accepted 12 July 2007
Available online 18 July 2007

Abstract

We describe a novel technique for improving the sensitivity of analytical instruments based on the measurement of fluorescent intensity. Independent measurement of the Rayleigh scattered intensity component by means of a second photodetector leads to normalized data, which are independent of various experimental parameters. Incorporation of this technique into a fully automated capillary waveguide biosensor improved the instrument sensitivity by a factor of three. The technique enables quantification, as well as detection, of the hybridized target molecules.
Published by Elsevier B.V.

Keywords: Deoxyribonucleic acid; Hybridization; Biosensor; Capillary; Fluorescence; Evanescent Wave

1. Introduction

Fluorescence based detection schemes are among the most sensitive analytical techniques for applications ranging from enhanced visualization in fluorescence microscopy, to DNA sequencing and biological/biochemical sensing [1,2], including sensors based on hybridization between a single-stranded nucleic acid "probe" and the nucleic acid "target" to be detected. The specificity of hybridization is controlled by well-established procedures, e.g. by adjusting probe sequence length. The probe is typically immobilized on a substrate, for example, an optical fiber or a planar waveguide [3–7]. In fluorescence-based hybridization sensors, target sequences are detected after hybridization to the surface-bound probe molecules. Depending on the strategy employed, hybridization can result in either an increase or a decrease in fluorescence relative to a zero-hybridization background level. Subsequent to detection, the probe-target hybrids are denatured by chemical means or through the use of elevated temperatures, allowing the sensor to be re-cycled for many hybridization/detection cycles. For natural samples, e.g. sea water, detection strategies can include competitive and/or complementary hybridization protocols [8–10], or the use of molecular beacon probes that fluoresce upon hybridization [11].

Detection of a hybridization event is achieved when the measured fluorescent intensity goes outside the bounds of a defined zero-hybridization threshold condition. This is a much less challenging problem than achieving absolute concentration measurements based on fluorescence intensity. Many experimental parameters cannot be reproduced between measurements taken at different times; i.e. the concentration versus fluorescence calibration curve is likely to change between uses of an instrument. Even in a perfect instrument, the quantum yield of different batches of the same dye will result in variation of fluorescent intensity that is unrelated to concentration. Such problems are severe obstacles to meaningful comparisons of data coming out of different research laboratories. In response, NIST researchers [12] proposed the development of standard reference materials (SRMs) that could be used to inter-calibrate instruments and laboratories. SRMs are most useful when the same instrument is being used by different laboratories and measurements are relatively insensitive to experimental parameters. NIST researchers have also recommended the adoption of a universal measure of fluorescence intensity referred to as molecules of equivalent soluble fluorophore (MESF), and MESF-based SRMs have been used for many years [13]. The use of MESF standard

* Corresponding author. Tel.: +1 631 632 8396; fax: +1 631 632 8494.
E-mail address: dhadwal@ece.sunysb.edu (H.S. Dhadwal).

0003-2670/$ – see front matter. Published by Elsevier B.V.
doi:10.1016/j.aca.2007.07.033

reference materials requires adherence to strict experimental controls, specifically: (1) the measurements of the standard and the test solution must be performed in the same instrument; (2) the excitation spectrum of the fluorophores in the standard and test solution should match; and (3) the emission spectrum of the fluorophores in the standard and test solution should match.

Although SRMs have found widespread acceptance in such popular instruments as the flow cytometer, SRM materials are not particularly useful for other types of fluorescence sensors, including capillary waveguide biosensors (CWB) [1,14]. The latter type are subject to larger variability in experimental factors, in part because of the many optical interfaces. Furthermore, while continuous flow is possible in a hybridization-based instrument, it is wasteful of sample materials which are often both scarce and expensive to obtain. Consequently, stop-flow protocols are employed to achieve low-volume hybridizations with minimal sample loss per hybridization. In this interrupted flow regime, micro-bubbles are unavoidable and can have a deleterious affect on data reproducibility. For example, the intensity of the evanescent wave illuminating a region of the immobilized probe on the inner surface of the capillary is dependent on the mode field distribution inside the capillary wall and therefore is highly affected by micro-bubbles. MESF based SRMs are not useful when the microenvironment within the instrument is variable.

Despite the many challenges facing CWB developers, Dhadwal et al. [14] described a CWB which used the interior region of a capillary both as a hybridization reaction chamber and an optical waveguide. They showed that such a sensor could be recycled many times and had a minimum detectable concentration of 30 pg mL^{-1}. However, the fluorescence intensity measurements could not be used to reliably estimate the concentration of target in unknown samples. This manuscript describes a dual detector approach for increasing the reliability of concentration estimates obtained from fluorescent intensity, that is, the sensitivity of the sensor. For in depth analysis of the CWB and definitions of sensitivity and detection limits the reader is referred to our earlier manuscript [14].

2. Theoretical considerations

The ideal fluorescence experiment described by Gaigalas et al. [12] is depicted in Fig. 1a. Using their arguments it is possible to estimate the fluorescent intensity (photon flux) in term of experimental and molecular parameters. If a single photon detector is illuminated by the fluorescent photon flux emanating from the sensing volume then the average number of fluorescent photon counts $\langle n_F \rangle$ in time interval T is given by

$$\langle n_F \rangle = T \left[\int_\lambda \Phi_F(\lambda) Q(\lambda)\, d\lambda \right] \quad (1)$$

where $Q(\lambda)$ is the quantum efficiency of a photodetector, e.g. a photomultiplier (PMT). The fluorescent flux per unit wavelength per second $\Phi_F(\lambda)$, is given by

$$\Phi_F(\lambda) = \varepsilon c \phi(\lambda) R(\lambda) \int_v I_0(r) \Omega(r)\, dr \quad (2)$$

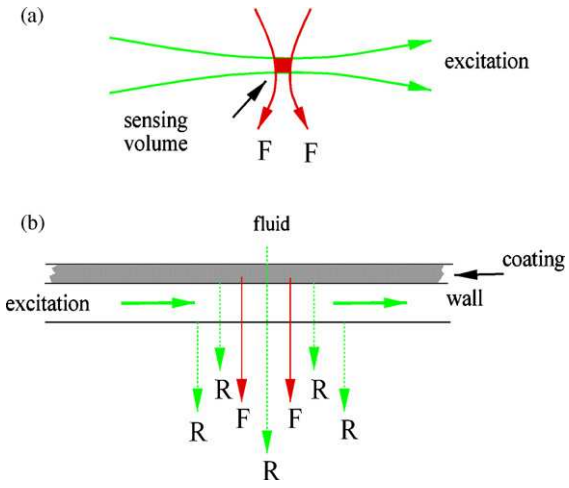

Fig. 1. (a) Ideal geometry for fluorescence detection; (b) CWS geometry. F—fluorescent photons and R—Rayleigh scattered photons.

where the integral is carried out over the sensing volume v, ε is the molar extinction coefficient ($m^2\ mol^{-1}$) at the excitation wavelength, c is the concentration of the fluorophore (mol L^{-1}), $\phi(\lambda)$ is the probability per wavelength of emitting a photon at λ, $I_0(r)$ is the photon flux ($m^{-2}\ s^{-1}$) at r, and $R(\lambda)\Omega(r)$ is the probability that a photon emitted at r will arrive at the PMT photocathode. It is assumed that the filter characteristics are the same for all paths through the collection optics. The factor $R(\lambda)$ defines the wavelength response of the various optical filters that separate the excitation component of the collected photon stream. The factor $\Omega(r)$ represents the spatial properties of the collection optics. Combining Eqs. (1) and (2) gives the fluorescence response of for the ideal instrument,

$$\langle n_F \rangle = T \left[\varepsilon \phi_0 \Omega \int_\lambda Q(\lambda) R(\lambda) s(\lambda)\, d\lambda \right] c. \quad (3)$$

where $\phi(\lambda)$ can be written as a product of the quantum yield ϕ_0 and a normalized spectral function $s(\lambda)$. The optical geometry factor Ω is defined by

$$\Omega \equiv \int_v I_0(r) \Omega(r)\, dr \quad (4)$$

Eq. (3) shows that the fluorescent intensity counts are proportional to the integration time T and the sample concentration c. The quantity in the square brackets corresponds to the slope of the concentration series. It should be noted that slope is a function of both the instrumental factors [$Q(\lambda)$, $R(\lambda)$ and Ω] and molecular factors [ε, ϕ_0 and $s(\lambda)$]. In order to obtain reliable fluorescent intensity measurements across different instruments or from repeated measurements with the same instrument, these factors must either be eliminated from consideration or be controlled with an appropriate calibration coefficient for instrument-independent measurements.

Gaigalas et al. [12] eliminated the consideration of these parameters by proposing the development of a set of standard solutions for use with identical instruments. Thus, for a particular instrument, the concentration of the test solution can be expressed as a ratio of the fluorescent counts for the test and stan-

dard solutions. The concentration of the test solution is expressed in MESF units. This protocol was developed with respect to the use of flow cytometers, which can be operated close to the ideal experimental conditions. Despite this, measurements of fluorescent intensity in terms of MESF units still have problems, as most fluorescence based instruments cannot be guaranteed to operate under the same conditions from to day to day. In particular, fluorescence sensors such as the CWB described by Dhadwal et al. [14] fall into this category of non-ideal field instruments, in which ideal behavior is traded for size, sensitivity and mobility.

Fig. 1b illustrates the optical geometry for the CWB. It is apparent that the geometrical factor Ω is far more complex than that of the ideal experiment. Specifically, the photons emanating from the sensing volume encounter three optical interfaces before being separated into the fluorescent and Rayleigh scattered components. The three interfaces are: (1) the fluid/coating; (2) the coating/capillary wall and (3) the capillary wall/air. On the excitation side, $I_0(r)$ is determined by the combined illumination arising from the evanescent wave field and the higher order, weakly guided modes in the interior region of the capillary. The former is strongly dependent on the properties of the three layer optical waveguide. Essentially, the strength and penetration depth of the evanescent wave field is a function of the modal distribution inside the wall of the capillary. The evanescent wave field can be influenced by small perturbations in the waveguide parameters. For example, the appearance of micro-bubbles at the coating/fluid interface can have a strong affect on the excitation intensity. The source of the micro-bubbles is not easily identified and due to its random nature is difficult to control reliably. Thus, the factor Ω in Eq. (3) is subject to erratic behavior for CWB systems, presenting a serious problem for obtaining consistent measurements of concentration of fluorophores based on absolute fluorescent intensity. In general, the factor Ω can fluctuate during a single measurement, or between a series of repetitive measurements for the same sample. Consequently, absolute comparisons between data taken at different times are confounded by the random nature of these fluctuations.

Even in a well-behaved, idealized fluorescence experiment, the photon flux emanating from the sensing volume contains both fluorescent photons and scattered photons (Rayleigh scattering) [15]. Typically, the former component is separated through the use of optical filters described by $R(\lambda)$. In general, optical filtering has to be very intensive in order to extract the fluorescent emission at low concentrations of fluorophores. State-of-art systems boast sensitivities of a few pg mL^{-1}, but the reproducibility, due to the factors discussed above, is very poor. In principle, the random intensity fluctuations may be eliminated by normalizing the fluorescent intensity by an independent measure of the Rayleigh scattered background from the same sensing volume.

This manuscript describes a novel dual detector technique which substantially increases the reproducibility of the solute concentration estimates. Essentially, the two components of the photon stream are measured using independent photodetectors. As discussed above one PMT measures the time average estimate of the fluorescent intensity, while the second PMT measures the photon counts due to the Rayleigh scattering background from the same sensing volume. The average number of photons due to Rayleigh scattering is

$$\langle n_R \rangle = \tau T \Omega \tag{6}$$

where τ is an attenuation factor of a neutral density filter placed in front of the PMT. The outputs of the two PMTs are combined to yield an instantaneous normalization of the fluorescent counts given by

$$N_F(t) = \frac{\langle n_F(t) \rangle}{\langle n_R(t) \rangle} = \frac{1}{\tau} \left[\varepsilon \phi_0 \int_\lambda Q(\lambda) T(\lambda) s(\lambda)\, d\lambda \right] c \tag{6}$$

Eq. (6) shows that the dual PMT detection scheme eliminates the Ω dependence from the measurements. Any variable molecular factors still need to be controlled. We note that this approach also may be valuable in conventional fluorescence experiments.

The following section describes the implementation of this scheme in an automated capillary waveguide biosensor.

3. Experimental

3.1. Materials

For natural samples, we would use protocols designed to detect unlabeled natural targets, e.g. by capturing the targets with a specific probe and subsequently labeling them with a non-specific fluorescently-tagged secondary probe (i.e. complementary hybridization). However, for laboratory tests we employed direct hybridization of a pre-labeled target to a surface-mounted probe. A capillary coated with a DNA probe sequence is exposed to a solution containing a synthetic target with a complementary DNA sequence, tagged with fluorescent dye molecules. Hybridization time and temperature can be adjusted to explore the dynamics of detection. At the end of the hybridization cycle the target solution is replaced by hybridization buffer and the measured fluorescence intensity corresponds to the number of target molecules that bound to the immobilized probe. The capillary can be reused by removing the bound target through a denaturing step.

3.1.1. Capillary preparation

Synthesized probe DNA was immobilized on the interior surface of silica capillary tubes using the method of Kumar et al. [16]. The silanized probe, obtained by reacting (3-mercaptopropyl)trimethoxysilane with a 5′-thiol-labeled oligonucleotide probe (Oligos Etc., Inc., Wilsonville, OR) in acetate buffer, was covalently attached to a NaOH-activated glass surface. The method was modified for use with capillaries (i.e., solutions were injected into capillaries and drying times were lengthened as needed). Kumar's method leads to a streamlined procedure for rapidly preparing coated capillary tubes.

The EUB338 sequence, which targets 16 s ribosomal RNA of the phylogenetic domain Bacteria, was used for the probe. A complementary target sequence, labeled with the fluorochrome Alexa532 (Molecular Probes, Eugene, OR) was also purchased (Oligos Etc.) to test the biosensor's stability and responsiveness.

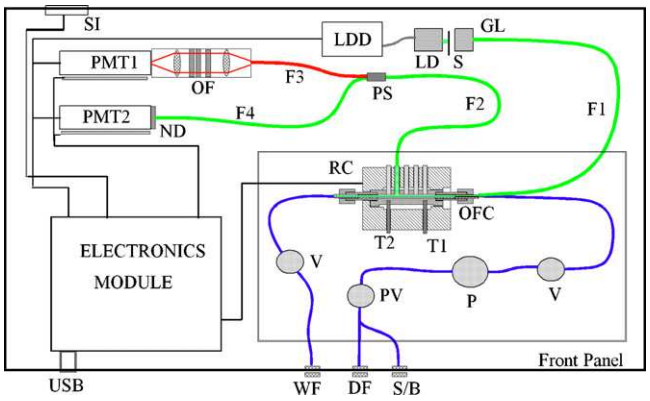

Fig. 2. Schematic of the CWB. WF—waste port for the fluid, DF—fluid port for denature solution, S/B—port for sample and buffer, can be connected to the carousel dip probe, PV—3-way pinch valve, V—isolation valves, P—micro-pump, T1 and T2 resistance thermistors, OFC—opto/fluid connector, RC—CWB housing, F1—illuminating optical fiber, F2—1 mm emission pick-up fiber, S—power splitter, F3—1 mm fiber, F4 – 110/140 μm fiber, OF—optical emission filter set, ND—neutral density filter, LDD—laser diode driver, LD—laser diode, S—shutter, OC—optical coupler, PMT1 and PMT2—photomultipliers, CR—control relays, USB—USB2.0 connector for PC, and SI—carousel interface connector.

3.2. Instrumentation

A CWB described by Dhadwal et al. [14] demonstrated that a hybridization reaction could be carried out in the interior region of a coated capillary. The sensor could be recycled many times after denaturing with formamide. A new fully automated CWB, which includes the dual detector approach discussed above, is shown diagrammatically in Fig. 2. The system is composed of four subsystems: (1) optical excitation and detection; (2) fluid control; (3) an electronics module; and (4) a graphical user interface (GUI) running on the host computer.

3.2.1. Optical excitation and detection

Excitation of the immobilized hybridized complex on the interior surface of the capillary is achieved through an opto-fluid connector (OFC) described by Dhadwal et al. [14]. Essentially, an optical connector (Amphenol #SMA 905) is modified to provide a fluid port in the central region, and a single or multiple fibers in the periphery of the connector for optical excitation and/or emission collection. Fluorophore molecules on the capillary wall coating or in the fluid stream can be illuminated directly by the weakly guided modes in the interior region of the fluid filled capillary, or indirectly by an evanescent wave field arising from the guided modes in the wall of the capillary. In order to implement the first method of excitation an opto/fluid connector, designated as T1, is used in which the transmitting optical fiber F1, is aligned parallel to the optical axis and illuminates the interior region of the capillary. Two alternative connector configurations (T2 and T3) position the transmitting fiber such that there is overlap with the capillary wall. T2 uses a 110/140 μm fiber whose dimensions are closely matched to capillary wall thickness of 150 μm, while T3 uses a 300/330 μm fiber such that some of the fiber core is also in contact with the fluid. The T2 illuminator exclusively excites the guided modes in the capillary wall, while the T3 illuminator includes additional excitation of some of the higher order, weakly guided modes in the interior region of the capillary.

An orthogonal geometry, which provides significant separation of the excitation source from the fluorescence emission, is used for capturing the photons emanating from the sensing volume. A 1 mm fiber, F2, with a numerical aperture of 0.48 (Thorlabs #URT1000) collects all of the emission emanating from the capillary surface. A special power splitter, PS, pipes most of the photons into a second 1 mm fiber, F3, which transports the photons, through collimating optics, a holographic notch filter (Kaiser #HNPF) and a band-pass emission filter (Omega Filters XF3074), OF, to a PMT (Hamamatsu model # H9305-04). Overall the out-of-band rejection is better than 10^{-5}. The second port of the power splitter is a 110/140 μm optical fiber, F4, which guides the photons through a neutral density filter, ND, to a second PMT, which provides the instantaneous photon counts corresponding to the Rayleigh scatter from the sample and the various optical interfaces.

A DPSS laser, LD (Photop Technologies model#GDL7020) is used for excitation of the Alexa 532 fluorophore used in the experiments reported here. The laser has a peak emission wavelength of 532 nm with a FWHM spectral width of 5 nm and delivers 15 mW of optical power. The laser is coupled into the transmitting fiber, F1, by means of a cylindrical gradient index lens, GL. In most cases excitation power is less than 1 mW. In order to prevent laser exposure during hybridization and minimize photobleaching, an electromechanical shutter, S, is activated only during measurement. Direct current modulation could not be used due to the warm up time required for this type of laser. Even after warm-up, the second-harmonic generation lasers, in the absence of active cooling, usually exhibit power fluctuations of about 20%.

3.2.2. Fluid control system

The fluid control system is designed for rapid mounting of the coated capillary tubes. A silica capillary tube (Polymicro Technologies #1.0/1.3 mm) is cut to a length of 65 mm and the two ends are mounted into half-inch long stainless steel sleeves. The ends are polished for optical flatness and, as discussed above, the capillary is subsequently processed for immobilizing probes on the interior surface. The capillary is easily mounted into a temperature-controlled housing, RC, made from copper and surrounded by an insulating shell made from black nylon thermoplastic. The capillary is held in place by means of SMA 905 optical connectors at either end of the housing. The connectors provide simultaneous fluid and optical access to the capillary.

Typically, several different fluids need to be pumped through the capillary during a hybridization cycle. Fluid flow is managed by a diaphragm micro-pump, P (Bio-Chem #120SPI12), two solenoid isolation valves, V (Bio-Chem #075T2NC12), and a 3-way pinch value, PV (Bio-Chem #075P3MP12). These fluid control devices are individually addressed through the GUI, which offers two modes of operation: manual and batch. The manual mode allows for full control of the fluid flow stream, while the batch mode enables unattended operation for processing twelve test samples. A carousel, with rotational and up-down

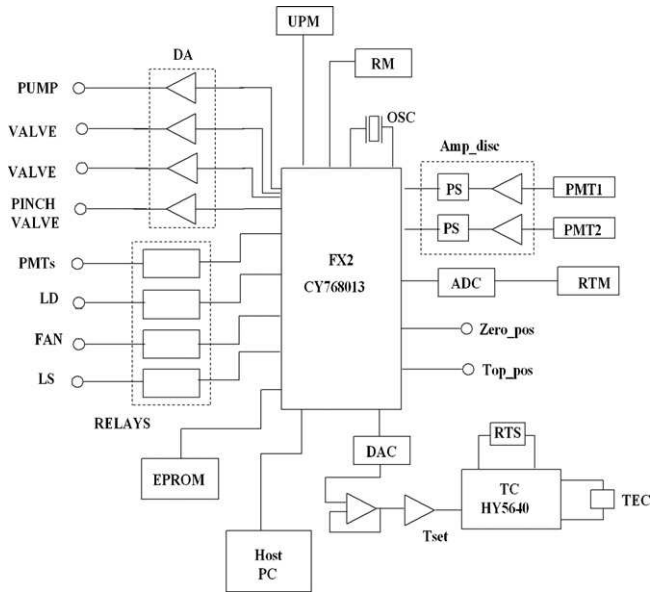

Fig. 3. Schematic of the electronics module controlling the CWB. DA—darlington amplifiers, DAC—digital to analog converter (Maxim 7545), ADC—analog to digital converter (Maxim 153), Amp-disc—amplifier discriminator for the photomultiplier (PMT), PS—pulse stretcher, OSC—oscillator, Zero_pos—zero position sensor, Top_pos—dip probe position sensor, RM—carousel rotary stepper motor, UPM—linear actuator for the dip probe of the carousel, RT—resistance thermistor, TEC—thermoelectric heat exchanger, T_{set}—set temperature.

stepper motors, uses a dip probe to access fluid in any of twenty-four 5 mL round vials. The user can easily program the CWB for unattended operation.

3.2.3. Electronics module

Fig. 3 shows a block schematic of the electronics module of the CWB. The entire control and data acquisition is designed around the Cypress FX2 (C67C68013), which integrates the USB 2.0 transceiver, SIE, enhanced 8051 micro-controller, and a programmable peripheral interface into a single chip. This is a very cost-effective solution that shortens development time and provides a small foot print for use in a mobile platform. Although not important in this application the FX2 can be operated at the maximum USB2.0 data rate of 45 Mbytes/s. The 8051 micro-controller runs software that can be downloaded to an internal RAM via the USB or from an EPROM (Atmel #24C164). Additionally, the 8051 has three high speed counter/timers which provide data acquisition and control of various components as discussed below.

Four high current relays (NEC #PS170A) are used to power up the PMTs, the laser diode, an optional fan for the temperature controller and the laser shutter. The 8051 generates the timing pulses for operating the self priming micro-pump, two isolation valves, and a 3-way pinch valve. External Darlington amplifiers, DA (Texas Instruments #ULN2003A), provide the current necessary to drive the pump and the valves. Batch operation requires the use of a carousel and a dip probe. The position and height of the dip probe are controlled by a motor, RM (Pik Power #SST42D1020) and the linear actuator, UPM (Herbach & Rademan #TM96MTR2873) both are powered directly from the FX2, via the 8051. Two optoelectronic interrupt switches provide the zero angle reference and the top of the fluid limit.

Temperature control of the fluid inside the capillary is attained through the use of a TEC (Melcor #CP1) heat exchanger using an analog controller from Hytek Devices (HY5640), which drives the current in a bipolar direction through the series of PN junctions until the set temperature is obtained. A sensing NTC thermistor, RTS (Betatherm #10K3A1IA) provides the requisite feedback. The operating temperature, in the range of 15–65 °C, is set by the user from the GUI application. A 8-bit digital-to-analog (Maxim 7545) converter inside the FX2 creates an analog voltage corresponding to the thermistor lookup table. A combination of an amplifier and transistor provide an active emulation of the set resistor, T_{set}, required by the Hytek controller, which uses proportional/integral control to attain temperature stability of 0.01 °C. However, due to the 8-bit digital-to-analog converter, the actual temperature stability is about 0.5 °C. A second thermistor, RTM, provides an actual measurement of the fluid temperature. The thermistor resistance is converted to a voltage drop, which is converted to 8-bit digital data by the analog-to-digital converter (Maxim 153). The GUI interprets the 8-bit word through another look-up table for continuous update of the fluid temperature display.

3.2.4. Graphical user interface

The graphical user interface (GUI) is designed to run on a Windows XP platform and is written in Visual C++. The GUI is used for the entire control of the instrument, including data logging, real time displays and post measurement playback feature to process archived data files. The sensor is controlled through a USB2.0 serial data interface. During normal operation three windows display the instantaneous count values of the Rayleigh signal, the fluorescent signal and the normalized signal. A fourth window displays the fluid temperature inside the capillary. The user is provided with full control of the experiment and full access to directory structure.

4. Procedures

4.1. Operation of the CWB

In the first series of experiments the efficacy of the normalization technique described above was investigated using an uncoated capillary and various concentrations of the Alexa532 fluorophore diluted in a hybridization buffer, whose composition was described Section 3.1.1. The T3 opto/fluid connector described above was used as the illuminator, with optical power of 0.6 mW emanating from the distal end of the fiber. In a typical run, a capillary was mounted into the CWB and loaded with the sample under test. A single measurement was taken over a time interval of 30–60 s, with data recorded every second. The single measurement can be repeated by reloading the sample. Thus, each run includes a series of measurement cycles. A new run is initiated with the re-mounting of the capillary and the opto/fluid connector. The measurement sequence was as follows: purge air to empty capillary; load 2 mL sample into the capillary; wait

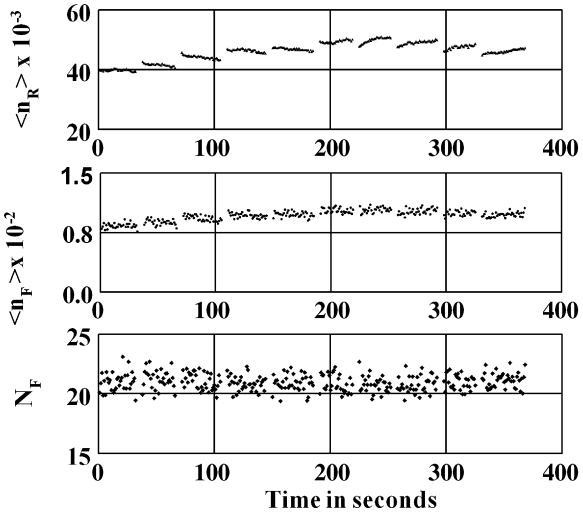

Fig. 4. Typical sensor output over one run.

60–120 s for fluid to reach set temperature; open the shutter for 30 s to acquire data.

Fig. 4 shows the measurements for one run of the uncoated capillary, which was re-loaded with the hybridization buffer before each cycle. The three traces represent, the Rayleigh scattered counts, the fluorescent counts and the normalized counts, respectively. The cycle to cycle value of normalized fluorescent intensity shows a reduced variation compared with the raw fluorescent signal. However, on occasions, the Rayleigh scattered counts will increase sharply, while the raw fluorescent counts do not follow, resulting in erroneous normalization. The source of the sharp changes in the Rayleigh scattered could not be isolated but it is conjectured to arise from the spontaneous generation of micro-bubbles in the field of view of the 1 mm collection fiber. However, this event is infrequent and easily detected.

Fig. 5 shows a summary of the data taken with a hybridization buffer. In order to assess the overall benefit of the dual detector technique, five different runs were performed. The following conclusions can be drawn from the data. First, the average signal-to-noise ratio of each 30 s measurement is 27.1 and 27.7 for the raw and normalized fluorescent data, respectively. This is an indication of the system stability during the 30 s interval and is expected to be the same for both measurements. Second, the relative deviation in the average value of the counts between cycles in one run is 12.6% and 6.7% for the raw and normalized fluorescent signals, respectively. Finally, the relative deviation between the cycles taken over the five runs is 17.9% and 6.3% for the raw and normalized estimates, respectively. These figures clearly confirm that instantaneous normalization, as discussed above, gives a significant improvement in the sensitivity of the fluorescent intensity data acquired with the dual detector approach.

Sensitivity and detection limits of the CWB were discussed in our previous manuscript [14]. The former is a measure of the repeatability of the sensor response while the latter is an indication of the lowest detectable target concentration. Ideally, a sensor with high sensitivity and low detection limit is desirable, however, a sensor with a low detection limit and a low sensitivity is still useful for target detection. The detection limit is not expected to change significantly from the previously reported value for the CWB, however, the sensitivity should be much higher. A reliable estimate of sensitivity can be obtained by repeated measurements of the sensor response over a range of target concentrations. Fig. 6 shows the results of a typical run, which includes a sequence of measurements of the various concentrations interlaced with measurements of the buffer. The lowest concentration of 27.6 pg mL^{-1} ($\sim 3 \times 10^{-12}$ M) is clearly detectable. At each concentration the solution was loaded twice, giving two 30 s independent measurements. The concentration series was repeated three times, for each of the opto/fluid connectors T1, T2 and T3 discussed above. Fig. 7 shows a concentration series summarizing these results. The error bars represent the variation in the normalized value over the three runs and two cycles per run, error bars smaller than the size of the symbol are not visible. The data has been further normal-

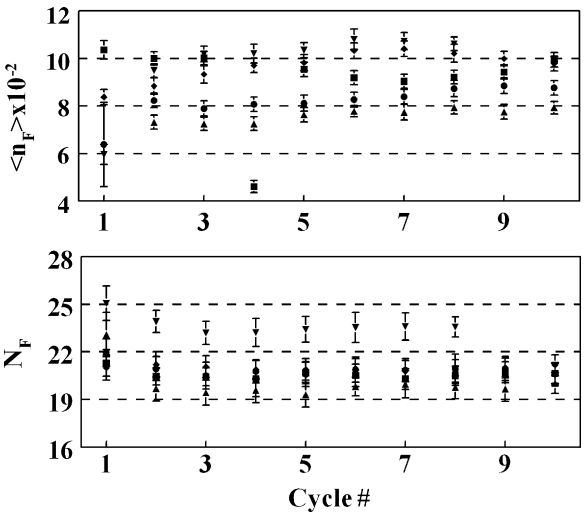

Fig. 5. Summary the fluorescent intensity data for the hybridization buffer. Five separate runs are indicated by different symbols. Each data point is the average of 30 points per cycle.

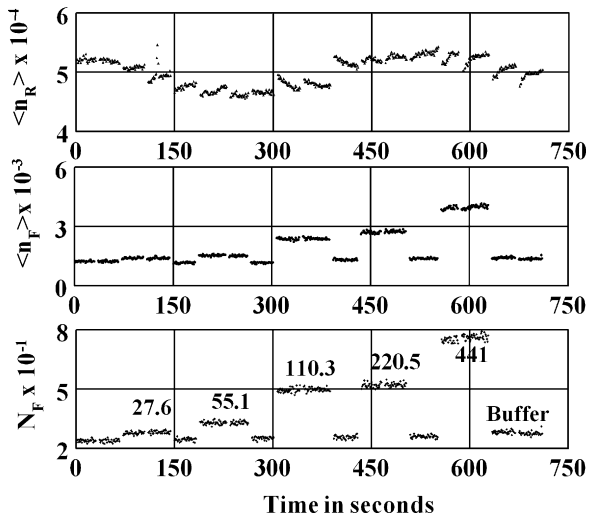

Fig. 6. Typical measurement over a range of dye concentrations (pg mL^{-1}). The lower panel is labeled with the concentrations in pg mL^{-1}.

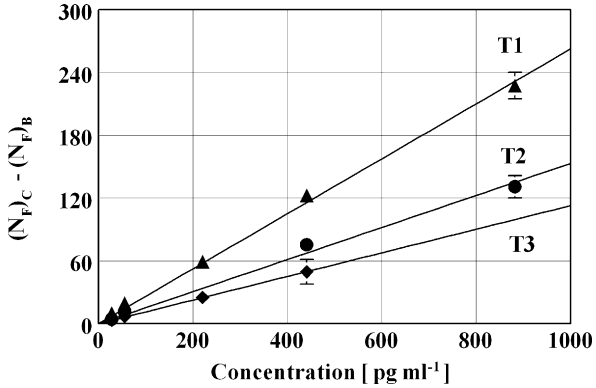

Fig. 7. Concentration calibration for the three opto/fluid connectors T1, T2 and T3. Each data point is averaged over three runs with two cycles per run.

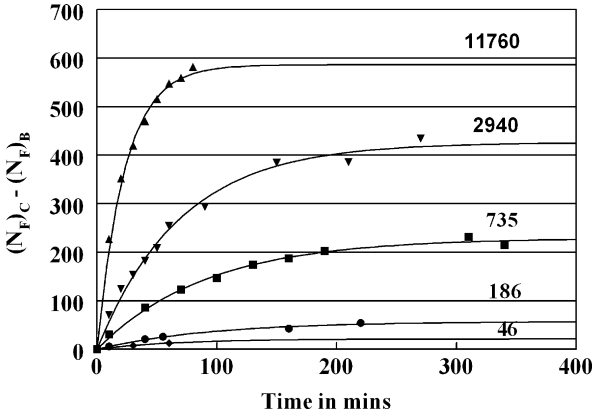

Fig. 8. Summary of hybridization kinetics using different concentrations of synthetic target. Annotations of concentration are in pg mL^{-1}.

ized by subtracting the average value of the normalized buffer for each of the illuminators. The graphs show a linear dependence between target concentration and normalized fluorescent intensity. Thus, it is possible to extract molecular concentration from the normalized fluorescence data taken at different times. As the error in concentration estimates decreases with increasing slope sensitivity, the T1 illuminator will give the smallest error in estimating concentration from the measured normalized value of fluorescent intensity. However, these graphs do not show that the T1 opto/fluid connector has two serious flaws: (1) extended exposure of the fiber surface to the fluid stream ultimately leads to failure of the opto/fluid connector; and (2) the problems associated with micro-bubbles are more probable. The significance of bubbles in capillary systems has been discussed by Wang et al. [17]. In the current design of the CWB, we find that the T3 illuminator is a better choice for extended use and reliable estimates of concentration from data taken at different times.

4.2. Hybridization and target concentration

Hybridization and denaturation measurements were performed at 40 °C using probe-coated capillaries. Typically, the capillary was loaded with the (nonfluorescent) hybridization buffer solution and allowed to equilibrate for 2 min before acquiring data, to ensure settling of micro-flows in the capillary. Fluorescence readings were recorded at 1 s intervals for 1 min. This procedure was repeated with several rinses of hybridization buffer until a stable baseline reading was achieved. A solution of fluorochrome-labeled target molecules in hybridization buffer was then injected. A 10-min hybridization time was typically used, in which target molecules bound to probe molecules immobilized on the interior capillary cell wall. The capillary was flushed with 5 mL buffer to remove unhybridized fluorescent probe, and reloaded with fresh buffer solution for fluorescence measurements. Following measurement, the hybridized target molecules were stripped from the probe molecules by filling the capillary with a denaturing solution (1:1 volume ratio of formamide and hybridization buffer) at 40 °C for 2 min. The capillary was then flushed, refilled with hybridization buffer, and the background fluorescence signal recorded.

Fig. 8 shows a summary of the rate of hybridization for several target concentrations. In all cases the sensor signal reaches a saturation level which is dependent on the target concentration. The underlying kinetics of hybridization, particularly for nuclei acids immobilized on a solid surface, are not well understood [18]. Given the abundance of probe in the immobilized state one might have expected all target concentration to eventually reach the same saturation level; this does not appear to be the case. Interestingly Ahn et al. [10] reported a very similar relationship for another type of biosensor.

The CWB response at concentration c can be modeled by a saturation value N_c and an equilibrium time constant τ_c, described by an exponential function,

$$N_F(t) = N_c \left[1 - \exp\left(-\frac{t}{\tau_c}\right)\right] \quad (7)$$

The solid lines in Fig. 8 show the results of a non-linear least squares curve fitting to the data using Eq. (7). From the fit parameters N_c and τ_c can be extracted and these are plotted in Fig. 9 as a function of concentration. The standard deviation of the fit parameters is indicated by the error bars, which are visible

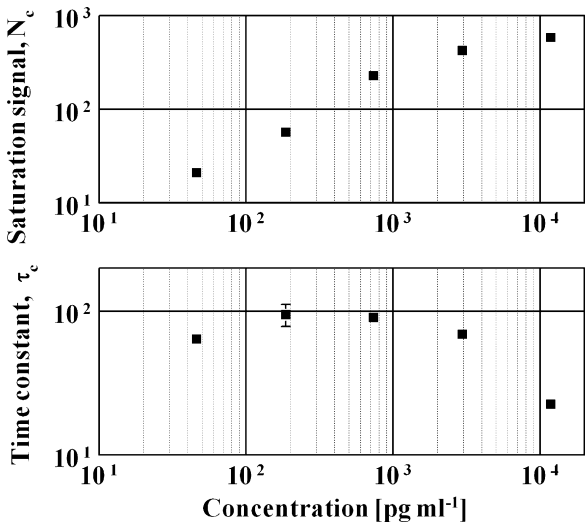

Fig. 9. CWB saturation signal and time constant for synthetic target. Error bars smaller than the symbol size are not visible.

only if the error is larger than the symbol size. The top panel in Fig. 9 shows the expected Beer's law relationship, that is, a linear dependence below a concentration of 1000 pg mL^{-1}. The lower panel shows that the relationship between the equilibrium time constant and the target concentration does not follow a simple linear law. However, this is to be expected if one can argue that the equilibrium time is a function of both the available probe and the target concentrations. Thus, the equilibrium time will be faster when either of the concentrations is more dominant and will exhibit a slower response when the ratio of the two concentrations is close to unity. A detailed study of the hybridization kinetics in capillary waveguide biosensors will be subject of future research.

5. Conclusion

We have demonstrated that Rayleigh scattering is an acceptable indicator of perturbations taking place in the micro-sensing environment of fluorescence based sensors. Instantaneous normalization of the fluorescent signal by the Rayleigh scattering background has proven to be an effective technique for enhancing the sensitivity of these sensors. In particular, a capillary waveguide biosensor using dual detectors provided consistent detection and quantification of the concentration of microbial targets in natural samples. Although not reported here, the CWB can be operated in a fully automated manner to analyze twelve samples using a carousel type handling system.

Acknowledgements

Support from NSF under contracts OCE-0352252 is appreciated. Kemp was supported through NSF Award EF-0424599 during analysis and preparation of this manu script.

References

[1] C.R. Taitt, G.P. Anderson, F.S. Ligler, Biosens. Bioelectron. 20 (2005) 2470.
[2] K.R. Rogers, Anal. Chim. Acta 568 (2006) 222.
[3] R. Bernini, N. Cennamo, A. Minardo, L. Zeni, IEEE Sens. J. 6 (2006) 1218.
[4] C. Mastichiadis, S. Kakabakos, I. Christofidis, M. Koupparis, C. Willetts, K. Misiakos, Anal. Chem. 74 (2002) 6064.
[5] E. Thrush, O. Levi, L. Cook, J. Deich, A. Kurtz, S. Smith, W. Moerner, J. Harris Jr., Sens. Actuator B-Chem. 150 (2005) 393.
[6] A. Lucotti, G. Zerbi, Sens. Actuator B-Chem. 121 (2007) 356.
[7] O. Leistiko, P. Jensen, J. Micromech. Microeng. 8 (1998) 148.
[8] Y. Wang, X. Wang, S.-W. Guo, S. Ghosh, BioTechniques 32 (2002) 1342.
[9] J. Medina-Sanchez, M. Felip, E. Casamayor, Appl. Environ. Microbiol. 71 (2005) 7321.
[10] S. Ahn, D.M. Kulis, D.L. Erdner, D.M. Anderson, D.R. Walt, Appl. Environ. Microbiol. 72 (2006) 5742.
[11] J. Lenaerts, H.A. Lappin-Scott, J. Porter, Appl. Environ. Microbiol. 73 (2007) 2020.
[12] A.K. Gaigalas, L. Li, O. Henderson, R. Voigt, J. Barr, G. Marti, J. Weaver, A. Schwartz, J. Res. Natl. Inst. Stan. 106 (2) (2001) 381.
[13] P. Kemp, S. Lee, J. LaRoche, Appl. Environ. Microbiol. 59 (193) 2594.
[14] H.S. Dhadwal, P. Kemp, J. Aller, M.M. Dantzler, Anal. Chim. Acta 501 (2004) 205.
[15] R.A. Mathies, K. Peck, L. Stryer, Anal. Chem. 62 (1990) 1786.
[16] A. Kumar, O. Larsson, D. Parodi, Z. Liang, Nucl. Acids Res. 28 (2000) e71.
[17] G. Wang, M. Lowry, Z. Zhong, L. Geng, J. Chromatogr. A 1062 (2005) 274.
[18] D. Erickson, D. Li, U.J. Krull, Anal. Biochem. 317 (2003) 186.